OPTIMIZATION OF POLYMER STAKE GEOMETRY BY FEA TO ENHANCE THE RETENTION FORCE OF AUTOMOTIVE DOOR PANELS

UDC:629.331:658.512.2
Original scientific paper https://doi.org/10.46793/adeletters.2025.4.2.3

R. Martínez-Hinojosa[1], J.E. Garcia-Herrera[2], I.E. Garduño[2], H. Arcos-Gutiérrez[2], M.G. Navarro-Rojero[3], V.H. Mercado-Lemus[4], J.A. Betancourt-Cantera[*4]

[1]Posgrado CIATEQ A.C., Western Industry Circuit Lot 11, block 3, No.11, Industrial Park, State of Mexico 52004, Mexico
[2]SECIHTI-CIATEQ A.C, Eje 126 No.225, Industrial Park, San Luis Potosi 78395, Mexico
[3]CIATEQ A.C, Retablo Avenue No.150, Constituyentes Fovissste, Queretaro 76150, Mexico
[4]SECIHTI-InnovaBienestar from Mexico, Science and Technology No.790, Saltillo 25290, Coah., Mexico

Abstract:
This study focused on optimizing retention geometries for automotive interior door panel assemblies using ultrasonic welding, a preferred technique due to its strength and clean aesthetic appearance. The research aimed to resolve the conflict between tight spatial constraints and the need to maintain structural integrity during side-impact collisions. Using a Design of Experiments approach based on the Taguchi L8 method, four key parameters were evaluated: height, length, number of reinforcements, and component clearance. Models designed in the computer and developed in Siemens NX were validated through finite element analysis to quantify stiffness, maximum retention force, and stress concentration using different ANSYS software. The optimized configuration – featuring a 10 mm height, 15.5 mm length, three reinforcements, and 0.5 mm clearance – increased strength by 33.8% (234.2 N vs. the traditional 175 N design) while reducing the required manufacturing area by 74%.

ARTICLE HISTORY
Received: 29 April 2025
Revised: 4 June 2025
Accepted: 16 June 2025
Published: 30 June 2025

KEYWORDS
Design optimization, Automotive industry, Standardized geometry, Ultrasonic welding, Finite element method, Retention force

1. INTRODUCTION

The automotive sector continues to evolve as manufacturers face increasing pressure to improve design efficiency, cut emissions, and adopt sustainable practices [1,2]. In response, key vehicle components are being redesigned, and advanced production methods are being introduced, particularly in interior door panel systems [3-5].

These components play a dual role; they must satisfy visual and design expectations while contributing to passenger safety by absorbing lateral impact energy during collisions. The panels are assembled using stakes specifically designed to hold the subassembly of the interior door panels. If these stakes do not maintain a minimum retention force between the plastic panel components, they can detach, potentially injuring the vehicle's occupants.

Additionally, optimizing the geometry of these components offers advantages such as size reduction, which in turn decreases weight by using less material in their production. Typically, these panels are constructed from polymer-based, multi-material assemblies. They are joined using mechanical fasteners, such as screws and clips, as well as more modern solutions, including stakes joined by ultrasonic welding [6-8].

Ultrasonic welding (UW) [9,10] is a method for joining thermoplastics; offering superior bond strength and a clean appearance without the need for adhesives or additional mechanical fixtures [11]. UW is a joining process that utilizes high-frequency mechanical vibrations to fuse materials, mainly

*CONTACT: J.A. Betancourt-Cantera, e-mail: jbetancourt@innovabienestar.mx

thermoplastics and metals, without requiring additional fluxes, adhesives, or fasteners. By applying ultrasonic vibrations (20–40 kHz) to the workpieces, localized frictional heat is produced at the interface, causing the material to melt and form a robust, permanent bond upon solidification [9]. These joining methods are vital for interior door panel subassemblies, where crash-resistant structural integrity is non-modifiable [12,13].

However, the geometric constraints imposed by miniaturization can modify manufacturing methods, assembly strategies, and equipment capabilities, often compromising the effectiveness of weld joints, creating an equilibrium between design aesthetics and functional performance [14]. These difficulties increase when adjusting scaling retention geometries. Increasing sizes may enhance mechanical strength, but they also limit design adaptability. Components could detach during impacts if not properly optimized, creating serious safety risks [15]. Current industry practice often defaults to conventional screw fastening for compact components, despite increased manufacturing complexity and costs [11].

An effective resolution requires concurrent engineering approaches that balance aesthetic intent with technical feasibility during early design phases. Post-design modifications lead to costly reengineering efforts and may compromise product performance [16]. This research specifically addresses the optimization of ultrasonic welding retention geometries for interior door panels, targeting maximum performance within stringent spatial constraints (15.5 mm × 9 mm × 15 mm) [14]. It is essential to note that efficiency is closely tied to optimizing the geometry of the stake. If the size of the stake is reduced, both the material volume and the area will be smaller than those of the original geometry. However, the key parameter that would see improvement is the retention force. Taking this into account and the dimensional restriction, it is expected that by optimizing the geometry of the stake, the retention force can be increased up to 201.25 N, which corresponds to an increase of 15% concerning the current geometry and that continues to comply with the INTSMT-40 internal standard (greater than 150 N), contributing to increasing the safety factor without capital investment or changes in the assembly strategy and methods.

The methodology integrates CAD modeling with finite element analysis (FEA), a computational technique critical for predicting structural behavior and optimizing automotive components [11,17-21]. This approach was utilized by Milojevic and Pesic [22], who investigated how increased mass and the specific installation of compressed natural gas (CNG) supply lines (from cylinders to a bus engine) affect stress concentrations. The study highlights the crucial role of finite element analysis (PAK software) in addressing automotive design challenges and validating structural integrity under extreme inertial loads. This procedure ensures structural integrity while minimizing detachment risks during collisions, with statistically validated performance parameters [5].

2. MATERIALS AND METHODS

The stake optimization methodology employed a systematic DoE approach to evaluate the critical geometric parameters that affect retention performance. The simulation was conducted on a workstation HPC (High-Performance Computer) with 192 cores. The software program used during the investigation was Siemens NX for design, Oasys PRIMER 19.0 for pre-processing (mesh, fixed load, boundary conditions, etc.), ANSYS LS-DYNA 12.2.1 for processing/solution (solving the equation system), i.e., the quasi-static simulation of the UW processes, and Beta CAE META 24.1 for result analysis. The study specifically investigated four key variables: stake height (h) (mm), stake length (l) (mm), number of reinforcement ribs (#), and component gap (δ) (mm). The parameters were selected based on an analysis of blade-type retention stake geometries in the automotive industry, based on manufacturer and supplier data regarding interior assemblies, as well as the most commonly used dimensional and retention characteristics (see Table 1). This study enabled the identification of the four critical variables governing design performance.

Table 1. Geometric dimensional parameters from comparable vehicle platforms

Geometric analysis								
Variable	#1	#2	#3	#4	#5	#6	Min. value	Max. value
Height (mm)	10	8.5	12	9.0	12.5	10.0	8.5	12.5
Length (mm)	8.0	7.5	15	10	17.0	7.5	7.5	17.0
Number of rib-type reinforcements	0	4	1	3	3	4	0	4
Gap between components (mm)	0.1	0.1	0.5	0.1	0.1	0.5	0.1	0.5

2.1 Considerations of the Model

Siemens NX software was utilized to create 3D models through computational modeling. The models comprised reinforcement structures optimized topologically, intricate curvature profiles that aligned with OEM requirements, and weld interface shapes that adhered to ultrasonic joining standards. Geometry simplification was utilized to prepare the CAD models for FEA, while maintaining essential features. Convergence was confirmed through adaptive meshing, and material properties were assigned using an isotropic thermoplastic framework. To create an accurate simulation, assembly constraints related to limitations were added. This methodology supports viable manufacturing processes and provides a measurable assessment of parameters such as structural rigidity (*K*) in N/mm, maximum retention force (*F_max* in newtons), localized stress amplification (*K_t*), and the reliability of weld cords under typical load conditions.

The integration of CAD and FEA can lead to optimized geometry of energy-directing features in ultrasonic welding applications that focus on thin-walled polymer assemblies in automotive interiors. The combination of technical precision in parameter specification and rigorous analytical methods results in manufacturable solutions that meet industry performance standards.

Fig. 1 displays the methodology used for geometric modifications, considering different control variables. Taguchi designed the L8 orthogonal array for four-factor experiments with two levels (maximum and minimum values). The L8 array limits the necessary combinations while still permitting an examination of the primary impacts of each factor, thus increasing the efficiency of the experiments. This considerably improves experimental efficiency, although it assumes minimal factor interactions [23,24]. To evaluate the significance of process parameters, the Taguchi method employs a statistical measure of performance called signal-to-noise. For this research, the noise factors or signals were: the stake material, mesh size, boundary conditions, and applied force speed. All these parameters remained constant throughout the simulation, which did not affect the results. Table 2 presents the design configuration, considering the control parameters identified in Fig. 1.

It is essential to conduct a structural analysis of geometry, considering it as a beam cross-section. In this case, the control parameters listed in Tables 1 and 2 were crucial.

The purpose of this evaluation is to ensure that the cross-section can withstand the imposed loads while still meeting the requirements for strength, stiffness, and stability. This process employs various analytical methods and verifications based on the principles of structural mechanics and established design standards.

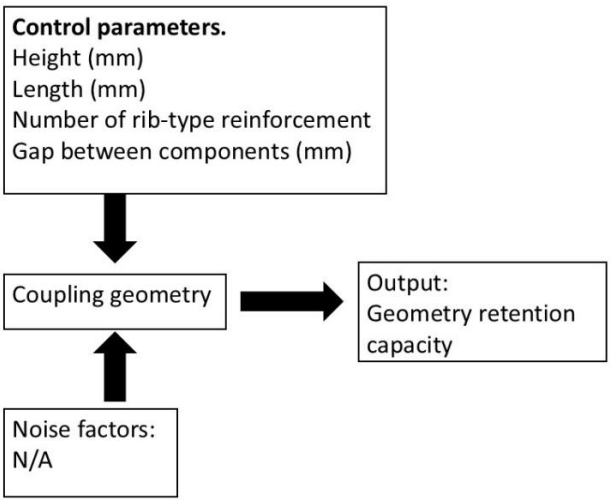

Fig. 1. Schematic of geometric control parameters for stake optimization

Fig. 2a) illustrates the traditional stake geometry used in the current assembly of side door interior panels before ultrasonic welding, while Fig. 2b) shows the resulting geometry after welding. Notably, the retention force analysis of this geometry measured 175 N.

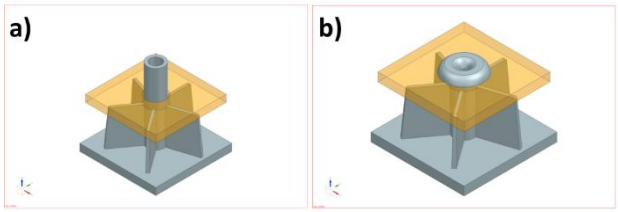

Fig. 2. Traditional coupling geometry, a) pre-welding and b) post-welding

3. RESULTS AND DISCUSSION

Based on the information in Tables 1 and 2, the control parameters for creating distinct geometric configurations are established, with each dimension limited to a specific operational range. The height parameter ranges from a lower bound of 8.5 mm to an upper bound of 12.5 mm, while the length covers a broader range from 7.5 mm to 17.0 mm. Structural reinforcement is applied in a binary manner, using either zero or four rib elements. Component clearance is inversely related, with tolerance boundaries set at 0.5 mm and 0.1 mm.

Table 2. L8 array for 4-factor experiments with 2 levels (maximum and minimum value shown in Table 1)

Array number	Height (mm)	Length (mm)	Interaction 1	Number of rib-type reinforcements	Interaction 2	Interaction 3	Gap between components (mm)
1	8.5 ^{L}	7.5 ^{L}	1 ^{L}	0 ^{L}	1 ^{L}	1 ^{L}	0.1 ^{L}
2	8.5 ^{L}	7.5 ^{L}	1 ^{L}	4 ^{H}	2 ^{H}	2 ^{H}	0.5 ^{H}
3	8.5 ^{L}	17.0 ^{H}	2 ^{H}	0 ^{L}	1 ^{L}	2 ^{H}	0.5 ^{H}
4	8.5 ^{L}	17.0 ^{H}	2 ^{H}	4 ^{H}	2 ^{H}	1 ^{L}	0.1 ^{L}
5	12.5 ^{H}	7.5 ^{L}	2 ^{H}	0 ^{L}	1 ^{L}	1 ^{L}	0.5 ^{H}
6	12.5 ^{H}	7.5 ^{L}	2 ^{H}	4 ^{H}	2 ^{H}	2 ^{H}	0.1 ^{L}
7	12.5 ^{H}	17.0 ^{H}	1 ^{L}	0 ^{L}	1 ^{L}	2 ^{H}	0.1 ^{L}
8	12.5 ^{H}	17.0 ^{H}	1 ^{L}	4 ^{H}	2 ^{H}	1 ^{L}	0.5 ^{H}
*Where L - denotes Low level and H - indicates High level							

Fig. 3 presents a comparative analysis of the geometric configurations evaluated in the DoE. The study reveals that geometries 1 and 2 (Figs. 3a and 3b) share the same base parameters – height of 8.5 mm, length of 7.5 mm, and no reinforcements – but differ only in their component clearance specifications.

In contrast, geometric 3 and 4 (Figs. 3c and 3d) show significant geometric differences due to an increased length of 17.0 mm and the addition of four structural ribs. This illustrates the extensive dimensional and topological variations achievable within the defined parameter space. In Figs. 3e and 3f, the geometries differ from those in Figs. 3c and 3d in that the height was increased from 8.5 mm to 12.5 mm, while the stake length was reduced from 17.0 mm to 7.5 mm. Additionally, in Figs. 3g and 3h, geometries were designed without rib reinforcements. These geometries maintained a height of 12.5 mm and a length of 17 mm, accounting for two levels of clearance between components: 0.1 mm and 0.5 mm.

The structural analysis of each geometric configuration treated the stakes as cantilever beams, focusing particularly on their cross-sectional properties. Fig. 4 compares two of the analyzed geometries (previously shown in Fig. 3). Key dimensional characteristics include a uniform thickness and height of 1 mm for all ribs (Fig. 4a) and an identical thickness of 1 mm for the main stake body (Fig. 4b). These standardized dimensions allowed for a consistent comparative evaluation of mechanical performance under load.

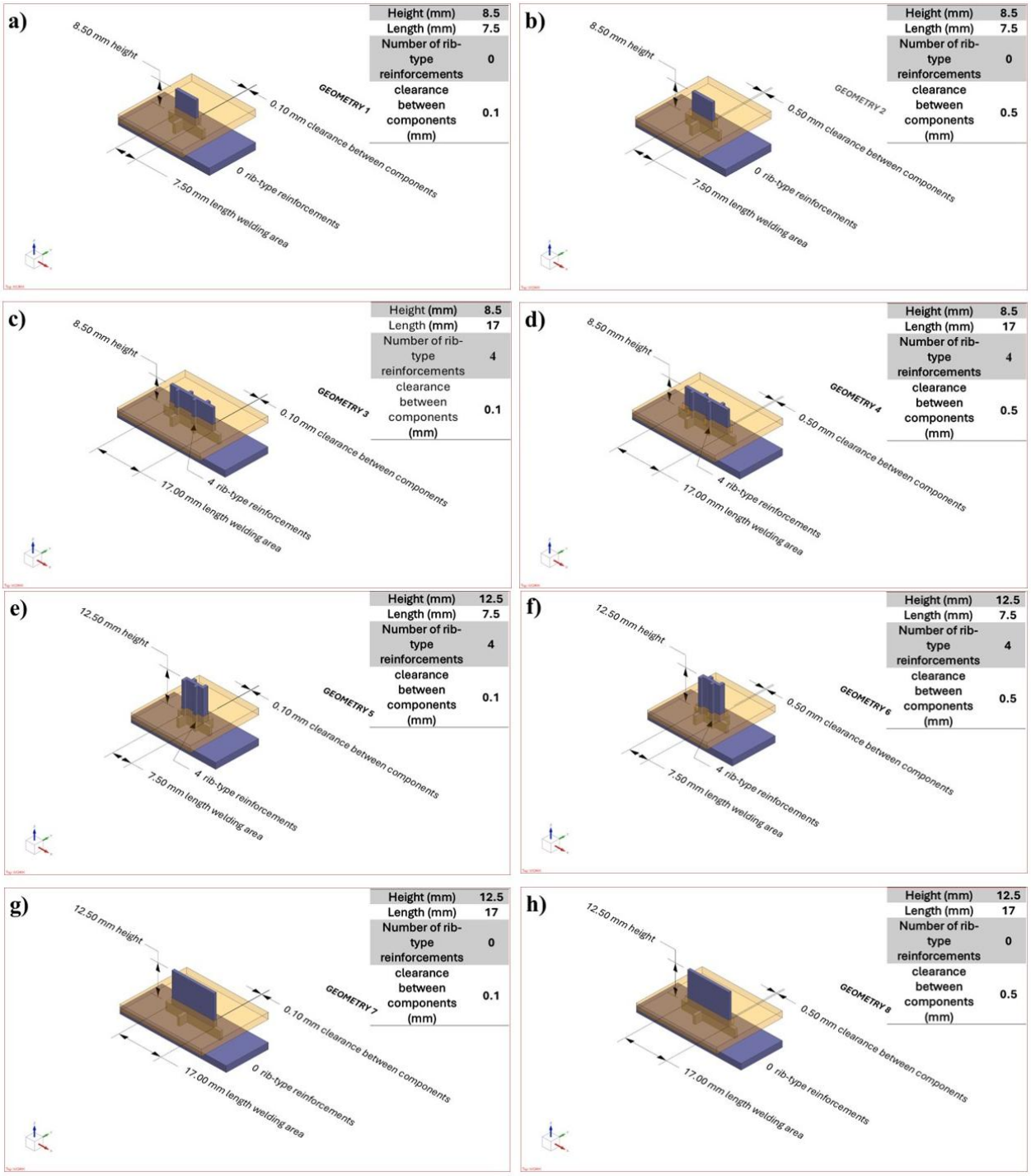

Fig. 3. Stake designs defined by the parameters of the DoE based on the maximum and minimum values provided in Tables 1 and 2. These geometries are: a) geometry 1, b) geometry 2, c) geometry 3, d) geometry 4, e) geometry 5, f) geometry 6, g) geometry 7, and h) geometry 8

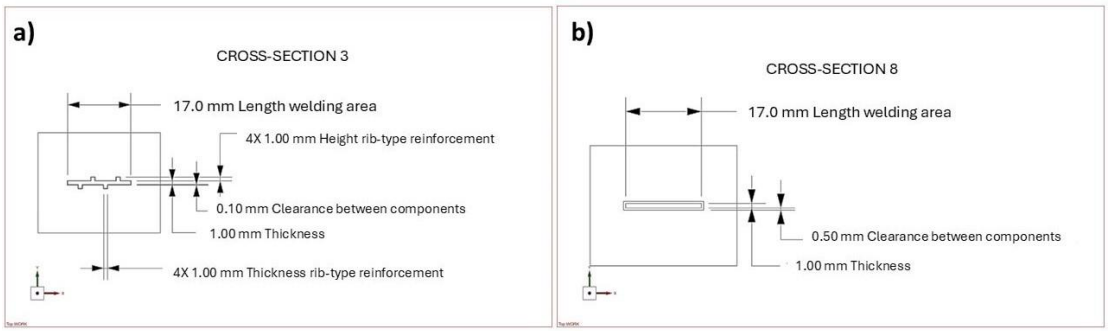

Fig.4. Cross-section of the analyzed stakes as beams

Fig. 5 shows a displacement curve obtained from a CAE simulation during the application of load on stake number 3. The plot displays the load capacity versus time during quasi-static testing. The maximum value on the Y-axis corresponds to the maximum supported load, a parameter used to determine structural limits and validate the performance compliance of each geometry. In this case, stake geometry number 3 demonstrates a maximum load capacity of 433.8 N.

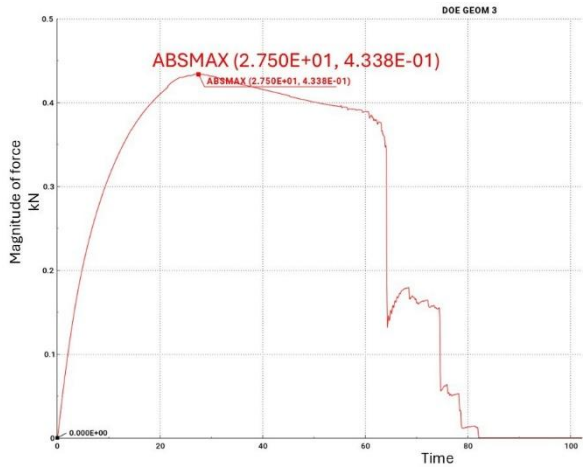

Fig. 5. Magnitude of the retention force for geometry 3

Fig. 6 summarizes the retention performance across all tested stake geometries, with data derived from load-displacement curves. After comparing the different designs, it was found that the third configuration delivered the strongest retention, measuring 433.8 N, while the fourth design followed with 405.7 N.

This improved performance appears to be related to the dimensions specified in Fig. 2: a vertical size of 8.5 mm, a length of 17 mm, and the addition of four reinforcing ribs, which contribute to its overall strength.

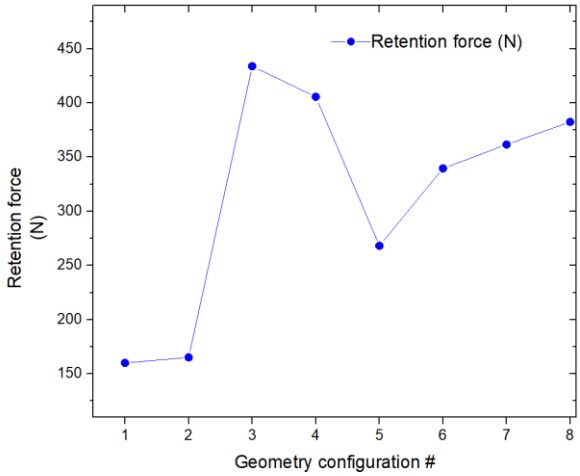

Fig. 6. Summary of retention curve values for each geometry type

The main distinction between them lies in the clearance between components—geometry 3 had a tighter fit at 0.1 mm, while geometry 4 used a 0.5 mm gap. This difference appears to play a decisive role in enhancing the mechanical locking behavior.

On the other hand, the following configurations demonstrated a gradual decrease in the retention force. For geometries 8 to 5, the measured values were 382.5 N, 361.6 N, 338.6 N, and 268.2 N, respectively. Meanwhile, geometries 1 and 2 demonstrated the poorest retention capabilities, measuring just 160.1 N and 165.2 N, respectively.

Clearly, the most effective geometries are found at the extremes of the dimensional ranges established by the DoE, indicating that maximum efficiency may be attained at the boundary limits of specific design parameters.

The graph presented in Fig. 7 depicts the main effects analysis of the variables examined in the experimental design. It illustrates the relationship between the levels of each variable and the studied response, specifically the maximum load supported. The slopes of the lines indicate both the magnitude and direction of each variable's effect: a steep slope signifies a significant impact, while a flatter line suggests a minor effect.

Among the variables analyzed, stake length had the most substantial impact on improving retention force, as supported by the previous Figure, which shows geometries 3 and 4 with a length of 17 mm. Conversely, the lowest retention values were observed in stake geometries designed with a length of 7.5 mm for designs 1 and 2.

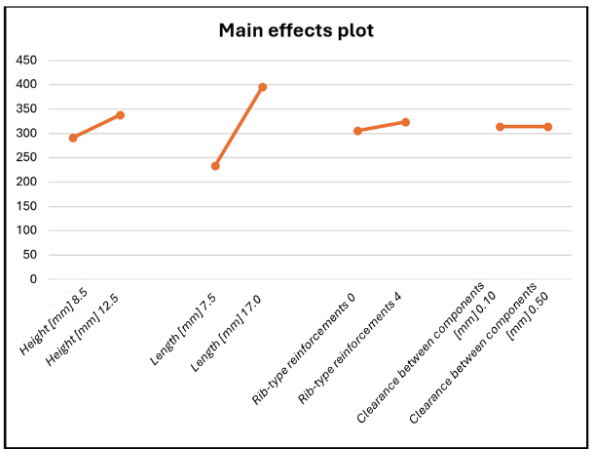

Fig. 7. Main effects plot from the experimental design

The following variable with the most significant influence, according to Fig. 3, corresponds to heights of 8.5 mm for the low level and 12.5 mm for the high level. The third variable with the least effect is the number of reinforcements.

Fig. 8 displays the optimized geometric design achieved through a multiparameter optimization process. This process evaluated dimensional constraints, reinforcement density, and component clearance to improve structural integrity and functional performance.

In Fig. 8a, the final stake geometry incorporates critical dimensions of 10.0 mm in height, 1.0 mm in thickness, 15.5 mm in length, and 8.1 mm in width. The dimensions were selected according to the structural performance and the cost of the material. This design incorporates three support ribs with a thickness of 0.55 mm. These ribs contribute to an increase in the structure's stiffness and promote the distribution of internal stresses, reducing the probability of premature failure. To ensure the dimensional tolerances required during assembly, a clearance of 0.50 mm was defined between components, as depicted in Figs. 8b and 8c. Additionally, Fig. 8d provides a simulation picture of the ultrasonic welding process, which is crucial for analyzing joint integrity and potential detachment scenarios.

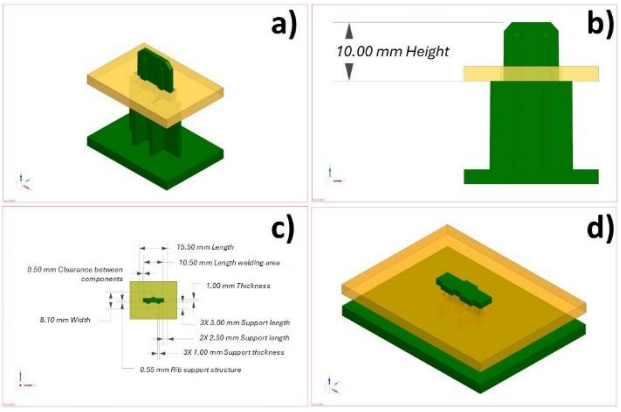

Fig. 8. Proposed standardized geometry showing pre-welding and post-welding configurations

Fig. 9 shows the results of tests focused on retention force. These tests were conducted under quasi-static conditions that simulate slow, progressive loads, utilizing a controlled convergent mesh and plastic strain failure criteria. These tests were performed using a step-by-step process using engineering simulation tools (CAE).

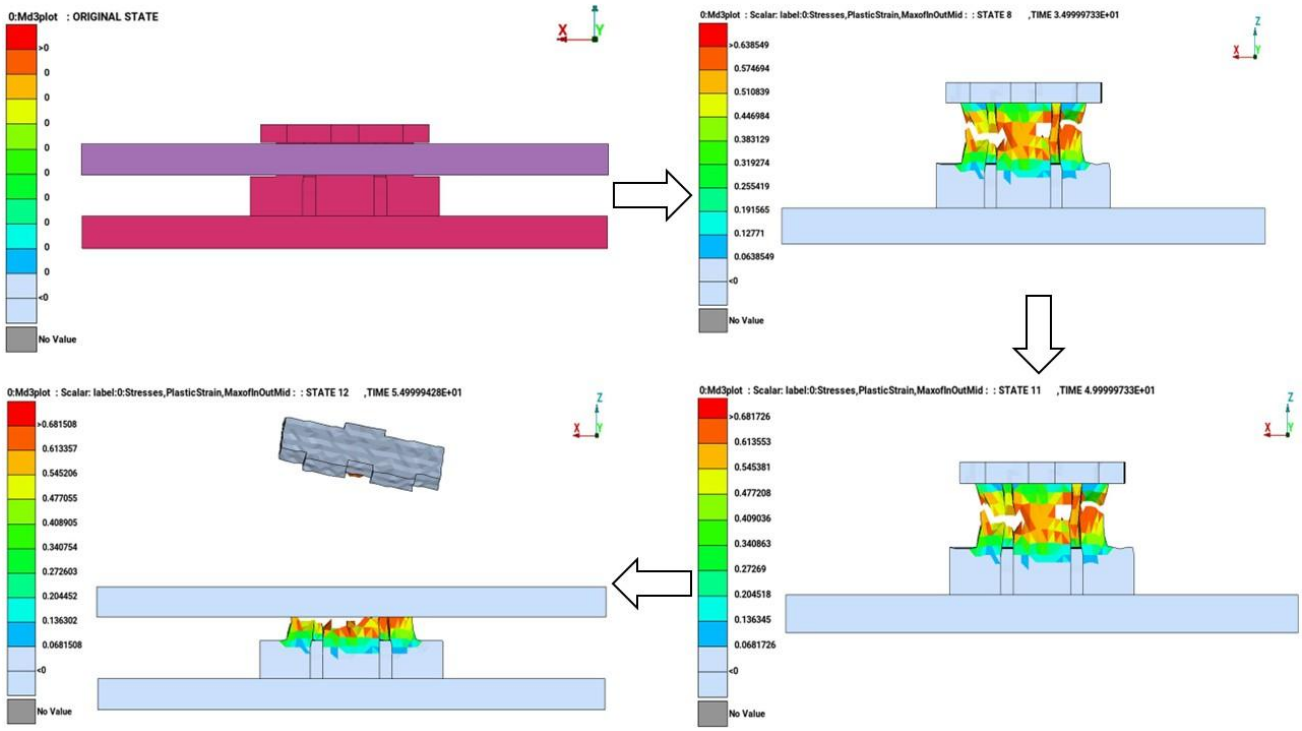

Fig. 9. Proposed geometry for standardization showing the sequence of CAE analysis

The results indicate that the chosen geometry maintains consistent performance under the expected loads and meets the required physical and dimensional standards. Additionally, the design aligns with production limitations, making it suitable for confined spaces in car interiors where strength and durability are essential.

Table 3 summarizes the findings from the simulation analysis, showing that the new geometry, considering the spatial constraints, achieves a retention force of 234.2 N. This value represents a 33.8% increase, and compared to the current geometry, which has a retention force of 175 N, this is approximately 56% more than the

requirement of the INTSMT-40 internal standard (greater than 150 N).

Table 3. Magnitude of the final proposal variables and their retention capacity

Tested values	Actual geometry	Optimized geometry	% of improvement
Retention force (N)	175	234.2	33.8%
Required area (mm^2)	484	125.55	74%
Required material volume (mm^3)	527.7515	271.7323	49%

On the other hand, compared to the range of different stake geometries used in the automotive industry, shown in Fig. 6, the value is 46.01% minor and 46.28% major the maximum and minimum retention force, respectively furthermore, the new design results in a 74% reduction in the required manufacturing area and a 49% decrease in volume.

4. CONCLUSION

Based on the analysis and development conducted in this research, the following conclusions were reached:

The optimization of the proposed geometries, guided by the design of experiments, resulted in eight design proposals that were analyzed to assess the retention force of each. The highest retention forces were recorded for geometries 3 and 4, yielding 433.8 N and 405.7 N, respectively. The only difference in comparing these two configurations was the gap between parts: geometry 3 incorporated a clearance of 0.1 mm, whereas geometry 4 had a gap of 0.5 mm. All other design parameters were kept identical. The main effects analysis indicated that length had the most significant impact on increasing retention force in the geometries, followed by stake height and the number of rib-type reinforcements. This analysis helped identify the optimal dimensions for achieving the best geometry design: 10 mm in height, 1 mm in stake thickness, 15.5 mm in length, 8.10 mm in width, 3 rib-type reinforcements, and a 0.50 mm intercomponent gap. These dimensions are subject to the established constraints of 15.5 mm in length, 9 mm in width, and 15 mm in height.

The validation of the simulated retention force in the ultrasonically welded stake yielded a value of 234.2 N, surpassing the current stake value used in the existing process. Furthermore, the new geometry enhanced the contact area and reduced the material volume required for manufacturing.

This study demonstrates that optimizing retention geometries for ultrasonic welding is achievable using CAD and FEA tools. The proposed geometry significantly enhances retention force and impact resistance, meeting the requirements of the automotive industry.

Acknowledgments

R.M.H. expresses gratitude to CIATEQ for the support provided during their master's studies in Advanced Manufacturing with an industrial focus. He also extends their appreciation to General Motors (GM) for facilitating the execution of this project.

The authors gratefully acknowledge the Support of the Investigadores por México-SECIHTI program through projects 850 and 674.

CONFLICTS OF INTEREST

The authors declare no conflict of interest.

REFERENCES

[1] L.E. Espino-De la Rosa, H. Arcos-Gutiérrez, J.E. García Herrera, I.E. Garduño, J.A. Betancourt-Cantera, Development of an innovative cooling system at the countershaft assembly station. *Applied Engineering Letters*, 9(4), 2024: 195–202. https://doi.org/10.46793/aeletters.2024.9.4.2

[2] Diálogo con la industria automotriz. *Asociación Mexicana de la Industria Automotriz*, 2012-2018. (In Spanish) https://www.amda.mx/wp-content/uploads/2018/02/Dialogos01-12-16.pdf (Access: 25 April 2025)

[3] O. Kıyılı, Plastic joining methods: Ultrasonic and vibration welding. *Uludağ Üniversitesi Mühendislik Fakültesi Dergisi*, 28(2), 2023: 665-684. https://doi.org/10.17482/uumfd.1278128

[4] J.O. Remigio-Reyes, I. Garduño, J.M. Rojas-García, H. Arcos-Gutiérrez, R. Ortigosa, Topology optimization-driven design of added rib architecture system for enhanced free vibration response of thin-wall plastic components used in the automotive industry. *The International Journal of Advanced Manufacturing Technology*, 123, 2022: 1231–1247. https://doi.org/10.1007/s00170-022-10219-x

[5] M.I.S. Chowdhury, Y.S. Autul, S. Rahman, M.E. Hoque, Polymer nanocomposites for automotive applications. In Advanced Polymer Nanocomposites; Eds. M.E.Hoque, Sharif, K. Ramar, A. Sharif. *Woodhead Publishing*, 2022: 267–317. https://doi.org/10.1016/B978-0-12-824492-0.00010-6

[6] S.K. Bhudolia, G. Gohel, K.F. Leong, A. Islam, Advances in ultrasonic welding of thermoplastic composites: A review. *Materials*, 13(6), 2020: 1284. https://doi.org/10.3390/ma13061284

[7] M. Uluskan, Decreasing defects in plastic injection molding and vibration welding processes through statistical process control. *Open Journal of Nano*, 6(2), 2021: 7–18.

[8] B. Patham, P.H. Foss, Thermoplastic vibration welding: Review of process phenomenology and processing-structure-property interrelationships. *Polymer Engineering and Science*, 51(1), 2011: 1–22. https://doi.org/10.1002/pen.21784

[9] S.A. Vendan, M. Natesh, A. Garg, L. Gao, Ultrasonic welding of polymers. In Confluence of multidisciplinary sciences for polymer joining. *Springer*, 2019. https://doi.org/10.1007/978-981-13-0626-6_3

[10] J.P. Davim, K. Gupta, Advanced welding and deforming. Handbooks in Advanced Manufacturing. *Elsevier*, 2021. https://doi.org/10.1016/C2018-0-00909-3

[11] P. Kah, L. Pavel, E. Hiltunen, J. Martikainen. Real-Time Weld Process Monitoring. *Advanced Materials Research*, 933, 2014: 117–24. https://doi.org/10.4028/www.scientific.net/amr.933.117

[12] D. Brassard, M. Dubé, J.R. Tavares, Resistance welding of thermoplastic composites with a nanocomposite heating element. *Composites Part B: Engineering*, 165, 2019: 779–784. https://doi.org/10.1016/j.compositesb.2019.02.038

[13] L.C.M. Barbosa, S.D.B. de Souza, E.C. Botelho, G.M. Cândido, M.C. Rezende, Fractographic evaluation of welded joints of PPS/glass fiber thermoplastic composites. *Engineering Failure Analysis*, 93, 2018: 172-182. https://doi.org/10.1016/j.engfailanal.2018.07.007

[14] I.F Villegas, R. van Moorleghem, Ultrasonic welding of carbon/epoxy and carbon/PEEK composites through a PEI thermoplastic coupling layer. *Composites Part A: Applied Science and Manufacturing,* 2018, 109, 75–83. https://doi.org/10.1016/j.compositesa.2018.02.022

[15] Z. Abbas, L. Zhao, J. Deng, S. Wang, W. Hong, Advances in ultrasonic welding of lightweight alloys: A review. *High Temperature Materials and Processes*, 42(1) (2023): 20220298. https://doi.org/10.1515/htmp-2022-0298

[16] C. Mandolfino, E. Lertora, C. Gambaro, Influence of cold plasma treatment parameters on the mechanical properties of polyamide homogeneous bonded joints. *Surface and Coatings Technology*, 313, 2017: 222–229. https://doi.org/10.1016/j.surfcoat.2017.01.071

[17] P.S. Kumar, Ch. Nagaraju, Weight optimization and finite element analysis of composite automotive drive shaft for maximum stiffness. *Materials Today: Proceedings*, 4(2), 2017: 2390–2396. https://doi.org/10.1016/j.matpr.2017.02.088

[18] D. Jankovics, A. Barari, Customization of automotive structural components using additive manufacturing and topology optimization. *IFAC-PapersOnLine*, 52(10), 2019: 212–217. https://doi.org/10.1016/j.ifacol.2019.10.066

[19] S.R. Kadam, P.D. Kale, Finite element analysis and optimization of automotive steering knuckle. *Journal of Interdisciplinary Cycle Research*, 12(7), 2020: 115–119.

[20] F.S. Chiwo, A.d.C. Susunaga-Notario, J.A. Betancourt-Cantera, R. Pérez-Bustamante, V.H. Mercado-Lemus, J. Méndez-Lozoya, G. Barrera-Cardiel, J.E. García-Herrera, H. Arcos-Gutiérrez, I.E. Garduño, Design and Optimization of the Internal Geometry of a Nozzle for a Thin-Slab Continuous Casting Mold. *Designs*, 8(2), 2024: 2. https://doi.org/10.3390/designs8010002

[21] M.S. Ashraf, Weld defect analysis in a pressure pipeline using 2d axisymmetric finite element analysis in ABAQUS. *Advanced Engineering Letters*, 4(1), 2025, 37-43. https://doi.org/10.46793/adeletters.2025.4.1.5

[22] S. Milojevic, R. Pesic, Theoretical and experimental analysis of a CNG cylinder rack connection to a bus roof. *International Journal of Automotive Technology*, 13, 2012: 497−503. https://doi.org/10.1007/s12239−012−0047−y

[23] J. Antony, Design of Experiments for Engineers and Scientists, Second edition. *Elsevier*, 2014. https://doi.org/10.1016/C2012-0-03558-2

[24] P.J. Ross, Taguchi Techniques for Quality Engineering. *McGraw-Hill*, 1996.